# We are IntechOpen, the world's leading publisher of Open Access books Built by scientists, for scientists

**4,800**
Open access books available

**122,000**
International authors and editors

**135M**
Downloads

Our authors are among the

**154**
Countries delivered to

**TOP 1%**
most cited scientists

**12.2%**
Contributors from top 500 universities

CLARIVATE ANALYTICS BOOK CITATION INDEX INDEXED

WEB OF SCIENCE™

Selection of our books indexed in the Book Citation Index in Web of Science™ Core Collection (BKCI)

## Interested in publishing with us?
## Contact book.department@intechopen.com

Numbers displayed above are based on latest data collected.
For more information visit www.intechopen.com

15

# Reducibility of Ceria-Based Materials Exposed to Fuels and under Fuel/Air Gradients

Domingo Pérez-Coll[1], Pedro Núñez[2] and Jorge R. Frade[3]
[1]*Instituto de Cerámica y Vidrio (CSIC),*
[2]*Universidad de La Laguna,*
[3]*Universidade de Aveiro,*
[3]*Portugal*
[1,2]*Spain*

## 1. Introduction

Ceria-based materials have been extensively studied in recent years for their potential use as solid electrolytes for alternative solid oxide fuel cells (SOFC) concepts, with emphasis on intermediate temperature SOFCs (Steele, 2000), single chamber SOFC (Yano et al., 2007), etc. However, the decrease in the oxygen partial pressure exerted by the presence of the fuel increases the non-stoichiometry accompanied by the reduction of $Ce^{4+}$ to $Ce^{3+}$. In these cases, reducibility of ceria-based solid electrolytes is a critical limitation, mainly because this implies onset of electronic conductivity (Blumenthal & Hofmaier, 1974; Blumenthal & Sharma, 1975; Tuller & Nowick, 1977; Navarro et al., 1997) and corresponding risks of internal short circuiting and decrease in cell voltage. The reducibility of cerias is affected by trivalent additives and their contents (Wang et al. 1997; Wang et al. 1998; Kobayashi et al., 1999), altering the mixed transport properties under low values of oxygen pressure according to the defect chemistry models. However some discrepancies are found in literature regarding the level of oxygen losses as well as the electronic conductivity (Mogensen et al., 2000; Zachau-Christiansen et al., 1996). On the other hand, ceria and related materials are also promising catalysts, including use as SOFC anode components for hydrocarbon conversion (McIntosh & Gorte, 2004; Tsipis et al., 2004). Performance in these prospective applications is likely to be promoted by the redox behaviour of cerias. Thus, one has studied the onset of electronic conductivity of the most promising ceria-based materials $Ce_{1-x}Gd_xO_{2-0.5x-\Delta\delta}$ (CGO) and $Ce_{1-x}Sm_xO_{2-0.5x-\Delta\delta}$ (CSO), including its dependence on temperature and composition (Pérez-Coll et al., 2004; Abrantes et al., 2003). The impact of low temperature sintering with suitable additives on the onset of n-type contribution under reducing conditions has also been studied (Fagg et al., 2003). In this chapter the dependence on oxygen partial is revised in detail, and corresponding effects imposed by fuels such as hydrogen or methane are examined by taking into account thermodynamic correlations between oxygen partial pressure and fuel conditions. This is extended for fuel/electrolyte/air gradients, as expected for SOFC operation.

Ceria based materials also undergo significant chemical expansion upon reduction of $Ce^{4+}$ to $Ce^{3+}$, causing non negligible strain under reducing conditions and important chemically induced stresses under fuel/air gradients. Thus, one re-examined strain/stress effects on combining the dependence of oxygen stoichiometry on working conditions with reported results of chemical expansion coefficient and relevant elastic properties of ceria-based materials. This included: (i) chemical strain in ceria-based anode components, and its dependence on temperature, fuel composition and electrode overpotential; (ii) strain/stress effects on ceria-based electrolytes fuel/air gradients, and other conditions imposed by SOFC operation.

## 2. Changes in oxygen stoichiometry under reducing conditions

### 2.1 Defect chemistry

The ionic conduction character in ceria-based compounds is generated by the introduction of aliovalent cations in the $CeO_2$ fluorite structure giving rise to the creation of oxygen vacancies due to a charge compensation mechanism (Yahiro et al., 1989; Mogensen et al., 2000). In particular rare earth additives are commonly employed to produce oxygen vacancies according to:

$$Ln_2O_3 \xrightarrow{CeO_2} 2Ln_{Ce}' + V_O^{\bullet\bullet} + 3O_O^x \tag{1}$$

This combines with oxygen stoichiometry changes under low values of oxygen partial pressure, due to partial reduction of ceria as follows:

$$O_O^x + 2Ce_{Ce}^x \Leftrightarrow \frac{1}{2}O_2(gas) + V_O^{\bullet\bullet} + 2Ce_{Ce}' \tag{2}$$

the last relation assumes that electrons resulting from oxygen exchange are localized as trivalent cerium ions $Ce^{3+}$, (Panhans & Blumenthal, 1993; Steele, 2000; Mogensen, 2000) producing small polarons (Tuller & Nowick, 1977; Panhans & Blumenthal, 1993; Navarro et al., 1997). If we assume that there is no interaction between defects, the mass action law of Eq. 2 is expressed as:

$$K_R = \frac{[V_O^{\bullet\bullet}][Ce_{Ce}']^2 pO_2^{1/2}}{[O_O^x][Ce_{Ce}^x]^2} \tag{3}$$

The electroneutrality condition for the most relevant defects is expressed as:

$$2[V_O^{\bullet\bullet}] = [Ce_{Ce}'] + [Gd_{Ce}'] \tag{4}$$

The concentration of the small polarons $[Ce_{Ce}']$ is directly related to the changes in oxygen stoichiometry $\Delta\delta$ according to:

$$[Ce_{Ce}'] = 2\,\Delta\delta \tag{5}$$

Recombination of Eqs. 4-5 allows one to express the concentration of remaining defects as functions of the stoichiometric changes and of the fraction of trivalent additive (x) as follows:

$$[V_O^{\bullet\bullet}] = \Delta\delta + x/2 \tag{6}$$

$$[O_O^{x}] = 2 - x/2 - \Delta\delta \tag{7}$$

$$[Ce_{Ce}^{x}] = 1 - x - 2\,\Delta\delta \tag{8}$$

and the mass action constant can be expressed as:

$$K_R = \frac{4(\Delta\delta)^2\,(\Delta\delta + x/2)\,pO_2^{1/2}}{(2 - x/2 - \Delta\delta)(1 - x - 2\Delta\delta)^2} \tag{9}$$

Equation 9 has been deduced without any assumption concerning the dependence of oxygen stoichiometry on the oxygen partial pressure, and allows one to obtain the mass action constant as function of oxygen loss. On the other hand the mass action constant relates to corresponding thermodynamic changes as:

$$\ln K_R = \frac{\Delta S_R}{R} - \frac{\Delta H_R}{RT} \tag{10}$$

which allows the determination of the entropy ($\Delta S_R$) and the enthalpy change ($\Delta H_R$) of reduction (Eq. 2). For low changes in oxygen loss, the oxygen nonstoichiometry is mainly determined by the trivalent-additive content ($\Delta\delta << x$), which corresponds to the ionic domain in ceria-based compounds. This produces nearly constant values for the concentration of oxygen vacancies, and validates a simpler approximation of Eq. 9, as follows:

$$\frac{K_R\,(2\text{-}x/2)(1\text{-}x)^2}{2x} = (\Delta\delta)^2 pO_2^{1/2} \tag{11}$$

Recombination of Eqs. 5 and 11 supplies an expression for the dependence of polaron concentration on the oxygen partial pressure according to:

$$[Ce_{Ce}'] = 2\Delta\delta \approx K_R'\; pO_2^{-1/4} \tag{12}$$

Note that Eq. 12 fails for relatively high oxygen losses and corresponding changes in oxygen stoichiometry. On the other hand, for low values of trivalent contents and/or relatively high oxygen loss ($\Delta\delta >> x$) the dependence of polaron concentration as function of the oxygen partial pressure may converge to:

$$[Ce_{Ce}'] \approx K_R''\; pO_2^{-1/6} \tag{13}$$

### 2.2 Determination of the oxygen loss by coulometric titration

Changes in oxygen stoichiometry are often determined by coulometric titration (Ferreira et al., 2000; Tikhonovic et al., 2002; Abrantes et al., 2003) using the cell design shown in Fig. 1. The whole electrochemical system is composed by YSZ-components. A highly-densified YSZ-tube is sealed between two YSZ-sintered pellets obtaining gas tight conditions. Powders of the compounds are introduced in a Pt-crucible which is inserted in the electrochemical cell. The YSZ-tube and one of the YSZ-pellets possess symmetrical Pt-

electrodes in the internal and the external surfaces. When the electrodes of the tube are submitted to a voltage difference, with the internal electrode under cathodic polarisation, by means of Pt-wires attached to an external d.c. source, there is a flow of oxygen ions through the YSZ-ionic conductor from the inner chamber to the external atmosphere. In this process the YSZ-tube acts as an electrochemical pump to extract oxygen, thus decrease the oxygen partial pressure inside the chamber. This imposes reduction conditions on the ceria-based material (Eq. 2), and the extent of oxygen losses can be evaluated by integrating the electrochemically pumped current. The voltage drop between both terminals of an auxiliary resistance connected in series to the electrochemical pump account for the current by means of the Ohm's law ($I=V_R/R$).

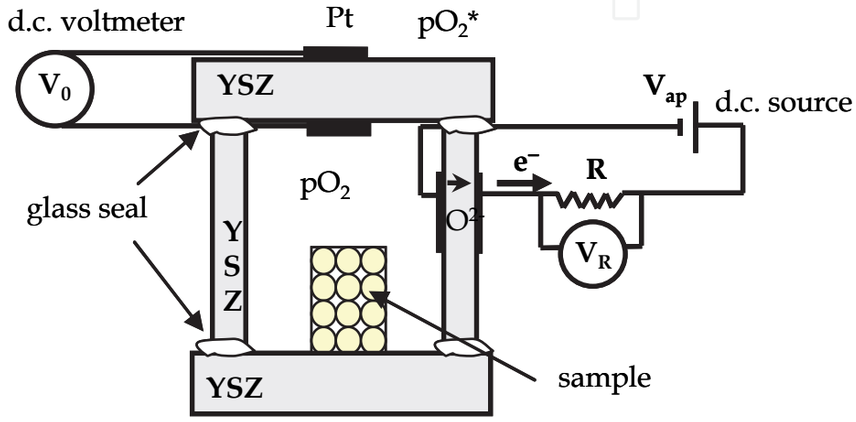


Fig. 1. Coulometric titration electrochemical cell used to determine changes in oxygen stoichiometry.

Pt-wires are also attached to the Pt-electrodes of the upper YSZ-pellet to connect to a d.c. voltmeter. In this situation the YSZ-pellet acts as a $pO_2$ probe and allows one to monitor the oxygen partial pressure inside the chamber by means of the voltage difference in both sides ($V_0$) according to the Nersnt equation:

$$V_0 = \frac{RT}{4F} \ln\left(\frac{pO_2^*}{pO_2}\right) \tag{14}$$

where F is the Faraday constant and $pO_2$* and $pO_2$ are the oxygen partial pressures of the outside atmosphere and of the inner chamber, respectively. The use of air as external atmosphere establishes $pO_2$*=0.21 atm. The experimental procedure consists in the application of several steps of potential to the pump, while recording transient changes until steady state conditions are restored. The overall molar amount of oxygen ($O_2$) extracted from the cell (chamber + stoichiometry change of the sample) between a generic step of applied potential is obtained by:

$$n_{O_2-\text{overall}} = \frac{1}{4F} \int_{t_1}^{t_2} (I(t) - I_\infty) \cdot dt \tag{15}$$

where $t_1$ and $t_2$ are the initial and the final times of the transient step, I(t) is the current through the electrochemical pump and $I_\infty$ is the residual current when the steady-state

condition is reached; this allows one to account for possible leaks. The molar amount of oxygen ($O_2$) corresponding to the gas phase of the chamber after a generic step of voltage between $t_1$ and $t_2$ is determined by:

$$n_{O_2-chamber} = \frac{pO_2(t_1) - pO_2(t_2)}{RT} \cdot V_{chamber} \tag{16}$$

where $V_{chamber}$ corresponds to the volume of the chamber after the subtraction of the volume of the sample and the crucible (Fig. 1), $pO_2(t_1)$ and $pO_2(t_2)$ correspond to the oxygen partial pressures at the starting and final steady-state situations. The oxygen stoichiometry change of the sample after a generic step is determined by:

$$\Delta\delta = 2\frac{M_{CLnO}}{m_{CLnO}}\left(n_{O_2-overall} - n_{O_2-chamber}\right) \tag{17}$$

where $M_{CLnO}$ and $m_{CLnO}$ are the formula weight and the mass of the sample. In the experimental procedure the voltage supplied to the pump is increased in steps of 50 mV, to analyze the change in oxygen stoichiometry as a function of the oxygen partial pressure. Figure 2 shows an example of two steps of applied potential to the electrochemical pump and the corresponding values of current and voltage of the electrochemical cell as function of time. The values of stoichiometry loss between two steps of equilibrium are determined by the numerical integration of current in the corresponding transient regime. Figure 3 shows the dependence of the oxygen loss on the oxygen partial pressure for $Ce_{1-x}Gd_xO_{2-0.5x-\Delta\delta}$ (x=0, x=0.1, x=0.2, x=0.3) at 1000 ºC and 800 ºC. Results reveal that there are important stoichiometry changes at low values of oxygen partial pressure which are clearly suppressed at lower temperatures, due to the decrease of equilibrium constant (Eq. 11). The extent of oxygen stoichiometry changes in ceria-based materials may account for significant oxygen storage ability with impact on catalytic or electrocatalytic processes.

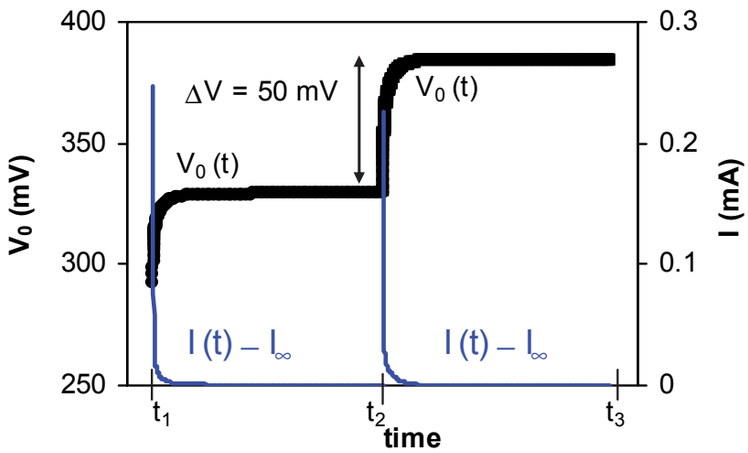


Fig. 2. Time dependence of current and voltage in the coulometric titration cell for two steps of applied potential from the d.c. source.

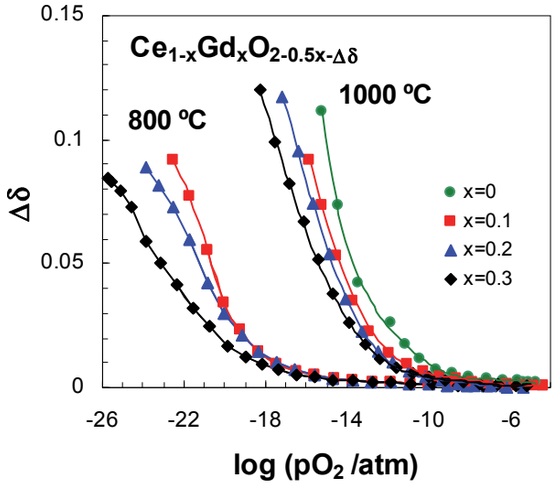


Fig. 3. Stoichiometry loss of $Ce_{1-x}Gd_xO_{2-0.5x-\Delta\delta}$ (x=0, 0.1, 0.2, 0.3) at 800 ºC and 1000 ºC as a function of the oxygen partial pressure.

Deviations from the nearly exponential behaviour are observed at very low values of oxygen partial pressure, mainly for lower temperature. An analogous behaviour was found by other authors (Riess et al., 1987; Panhans et al., 1993; Wang et al., 1998) and could be due to deviations from the simple defect chemistry model, or limitations of the experimental procedure. Though the steady state current $I_\infty$ should account for residual permeability through the YSZ cell components, this may not be the case for deviations from material/gas equilibrium or differences between the measured emf and the true conditions inside the cell. Figure 3 also shows that the introduction of the trivalent dopant ($Gd^{3+}$) in the $CeO_2$ fluorite structure decreases the reducibility and the effect is more pronounced for higher contents of dopant. Samples with higher contents of $Gd^{3+}$ possess higher concentrations of extrinsic oxygen vacancies (Eq. 1); this should decrease the reducibility of the compounds in order to preserve the equilibrium in Eq. 2. On the other hand, coulometric titration results could be conveniently treated (Abrantes et al., 2003) to obtain an estimation of the mass action constant according to Eq. 9, without any assumption concerning the dependence of the oxygen loss on the oxygen partial pressure; this is represented in Fig. 4 for $Ce_{1-x}Gd_xO_{2-0.5x-\Delta\delta}$ (x=0.1, x=0.2, x=0.3) at 800, 900 and 1000 ºC.

Fig. 4 shows that changes in stoichiometry do not produce considerable effects in the equilibrium constant. Deviations from the ideal model are mainly observed at lower temperature for sample with higher content of extrinsic vacancies (x=0.3), which could be related to defect interactions between oxygen vacancies and trivalent cations as $Gd^{3+}$ or even $Ce^{3+}$ (Schneider, 1997; Butler, 1983; Catlow, 1983; Minervini, 1999) probably because they are far from dilute conditions. Moreover, Fig. 4 shows similar values for samples with different contents of $Gd^{3+}$ as observed in Fig. 5 for the effect of temperature on the mass action constant. Typical values of enthalpy of reduction in the range 410-430 KJ/mol are extracted by using Eq. 10, which are comparable to other results reported in literature (Wang et al., 1997; Wang et al. 1998; Kobayashi et al., 1999; Kudo & Obayashi, 1976; Schneider et al., 1997). The simple defect chemistry behaviour can be used to model the theoretical dependence of oxygen loss on oxygen partial pressure (Eq. 9), allowing one to obtain the values of $K_R$ from experimental data (Fig. 4) and to use this to describe the dependence of

defect concentrations as ([$Ce_{Ce}^{x}$], [$Ce_{Ce}'$] and [$V_O^{\bullet\bullet}$]) on working conditions (Eqs. 5-8). This dependence is shown in Fig. 6.

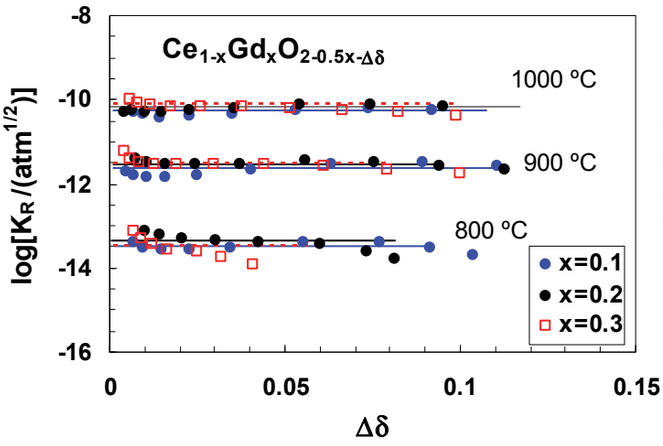


Fig. 4. Estimation of the mass action constant as a function of the oxygen loss for $Ce_{1-x}Gd_xO_{2-0.5x-\Delta\delta}$ (x=0.1, x=0.2, x=0.3).

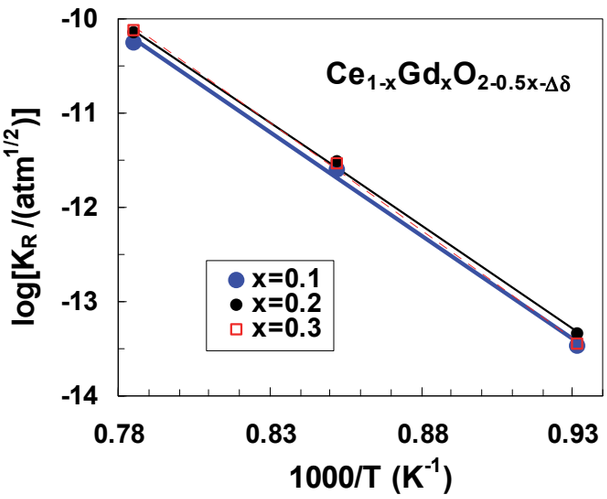


Fig. 5. Temperature dependence of the mass action constant for $Ce_{1-x}Gd_xO_{2-0.5x-\Delta\delta}$ (x=0.1, x=0.2, x=0.3).

The simple defect chemistry model seems to fit well experimental results for moderately reducing conditions, whereas deviations are observed for very reducing conditions, as previously mentioned. Though Eq. 9 was obtained without any *a priori* assumption concerning the dependence of defect concentration on the oxygen partial pressure, the

actual results still show transition for the dependence of log ([$Ce_{Ce}'$]) on log ($pO_2$) with -1/4 slope, for oxidizing conditions (Eq. 12), to -1/6 for very reducing conditions (Eq. 13).

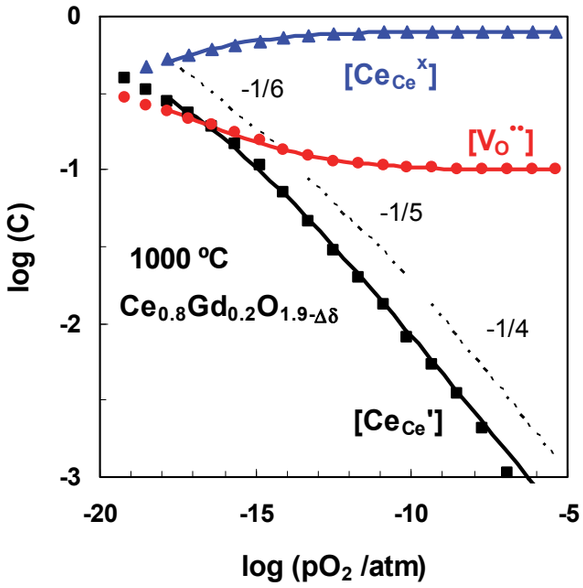


Fig. 6. Defect chemistry concentrations (molar fractions) as functions of oxygen partial pressure for $Ce_{0.8}Gd_{0.2}O_{1.9-\Delta\delta}$ at 1000 ºC. Single points correspond to the experimental values obtained from coulometric titration, whereas straight lines correspond to theoretical values using the simple defect chemistry model.

## 3. Electronic conductivity under reducing conditions

### 3.1 Theoretical analysis

The electronic transport in ceria-based materials is attributed to thermally activated-polaron hopping (Tuller & Nowick, 1977; Panhans & Blumenthal, 1993; Suzuki et al., 2002), and the electronic conductivity is expressed as:

$$\sigma_n = q_e \, n \, \mu_e \tag{18}$$

where $q_e$, n and $\mu_e$ are the charge, the concentration and the mobility of the electron. Since electrons are localized on trivalent cerium it is usually assumed that n= [$Ce_{Ce}'$], and mobility of electrons for the thermally activated polarons is expressed as follows:

$$\mu_e = \frac{\mu_{e,0}}{T} \exp\left(\frac{-\Delta H_m}{RT}\right) \tag{19}$$

where $\Delta H_m$ is the enthalpy of mobility of polarons. As noted by Navarro et al. (Navarro et al., 1997) the hopping conductivity should be proportional to [$Ce_{Ce}'$][$Ce_{Ce}^x$], which describes the probability of the small polaron to have a $Ce^{4+}$ as neighbour, and thus to provide charge transport. However, the mole fraction [$Ce_{Ce}^x$] is usually included in the mobility term. Under the assumption that the oxygen nonstoichiometry is determined by the trivalent content ($\Delta\delta << x$; Eqs. 11-12), the expression for electronic conductivity reads:

$$\sigma_n = \frac{\sigma_{e,0}}{T} \exp\left(-\frac{(\Delta H_m + \Delta H_R / 2)}{RT}\right) pO_2^{-1/4} \quad (20)$$

As consequence, the activation energy for hopping conduction is comprised of the enthalpy of mobility and half enthalpy of reduction.

### 3.2 Measurement of electronic conductivity by Hebb-Wagner ion-blocking

The determination of the electronic conductivity as function of the oxygen partial pressure requires a special procedure to separate the electronic and ionic contributions. The Hebb-Wagner procedure is a suitable technique based on blocking the transport of oxygen ions through the membrane submitted to a gradient of oxygen partial pressure (Hebb, 1952; Wagner, 1957; Navarro et al. 1997; Lübke & Wiemhoefer, 1999). For this purpose, symmetrical Pt-electrodes are placed on both surfaces of a gas tight ceria sample, and an alumina impervious disk is then sealed on one of the electrodes, avoiding oxygen leakage to the internal chamber (Fig. 7). Two Pt wires are attached to the outer electrode and another two wires are attached to the inner. One pair of these wires are connected to the d.c. source to supply the voltage difference between the inner and the outer electrodes, thus providing the oxygen partial pressure gradient, and the other pair is connected to a voltmeter to read the voltage difference in the pellet, acting as sensor of $pO_2$.

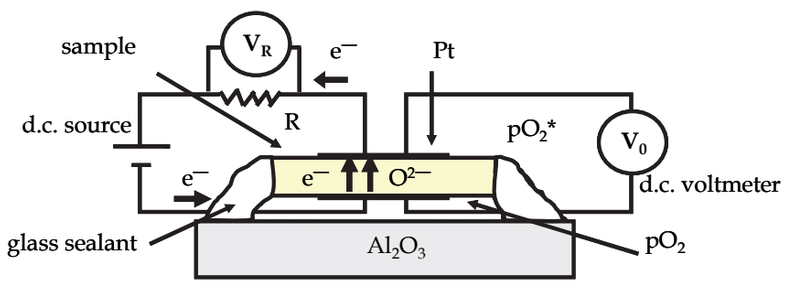


Fig. 7. Schematic view of the ion-blocking experimental setup.

When the internal electrode is cathodically polarized, oxygen ions flow through the membrane from the inner chamber to the outside atmosphere until steady-state conditions are reached. Since the blocking electrode prevents ion transport, the residual current reduces to the electronic contribution, after a transient regime (Fig. 8).

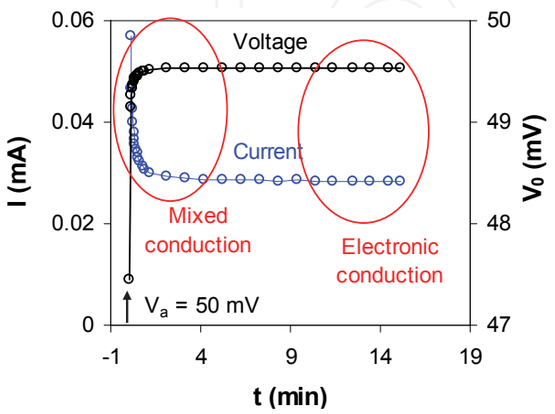


Fig. 8. Electrical current and voltage in the sample after applying a generic potential of 50 mV from the d.c. source.

The procedure includes application of cathodic voltages to the internal electrode from 50 to 1200 mV in steps of 50 mV, thus decreasing the oxygen partial pressure in the chamber from air to very reducing conditions. The voltage difference between the two electrodes is related to the oxygen partial pressure gradient by the Nernst equation (Eq. 14). An auxiliary resistance is connected in series to the sample and the d.c. source to account for the electrical current by means of the voltage drop at the former ($V_R$). Figure 9 shows the current-voltage curves of $Ce_{1-x}Gd_xO_{2-0.5x-\Delta\delta}$ (x=0, x=0.1, x=0.2, x=0.3) under the steady-state situation in ion-blocking conditions. The onset of electronic conduction is observed for moderate reducing conditions, and it is displaced towards more reducing conditions when the content of the trivalent-dopant increases, suggesting a decrease of the n-type electronic conductivity.

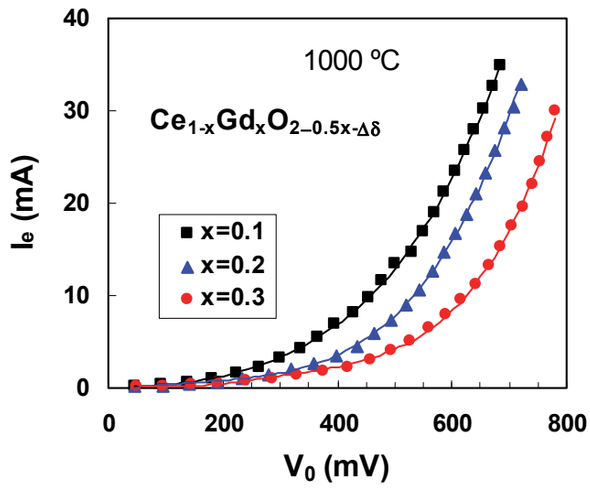


Fig. 9. Steady-state current-voltage for $Ce_{1-x}Gd_xO_{2-0.5x-\Delta\delta}$ (x=0.1, x=0.2, x=0.3) at 1000 ºC.

The electronic conductivity in the reduced side of the sample ($\sigma_e$) can be obtained by differentiation of the current against the voltage difference of the sample in steady-state conditions (Lübke & Wiemhoefer, 1999; Abrantes et al., 2003) according to:

$$\sigma_e = \frac{L}{A}\frac{dI_e}{dV_0} \tag{21}$$

where L and A are the thickness of the pellet and the area of the electrodes and $I_e$ and $V_0$ are the current (electronic current) and the voltage of the pellet in steady-state conditions (ion-blocking). Note that the differentiation performed to the voltage gradient across the sample is related to changes in the oxygen partial pressure in the side of the chamber. At relatively high values of oxygen partial pressure (moderate reducing conditions) the dependence of the n-type electronic conductivity on the oxygen partial pressure could be assumed to follow a -1/4 single power law (Eq. 20). In similar conditions, the p-type electronic conductivity could be assumed to follow a +1/4 power law as function of the oxygen partial pressure (Panhans & Blumenthal, 1993), yielding the following dependence for total electronic conductivity:

$$\sigma_e = \sigma_n^* \left( \frac{pO_2}{pO_2^*} \right)^{-1/4} + \sigma_p^* \left( \frac{pO_2}{pO_2^*} \right)^{1/4} \quad (22)$$

where $\sigma_n^*$ and $\sigma_p^*$ are the n-type and p-type electronic conductivities at the reference oxygen partial pressure ($pO_2^*$). Recombination of Eqs. 14 and 22 yields the following relation between electronic current and applied voltage (Navarro et al. 1997):

$$I_e = \frac{ART}{FL} \left\{ \sigma_n^* \left[ \exp\left( \frac{FV_0}{RT} \right) - 1 \right] + \sigma_p^* \left[ 1 - \exp\left( \frac{FV_0}{RT} \right) \right] \right\} \quad (23)$$

Experimental results were also fitted to Eq. 23 to show that this approximation is only acceptable for oxidising or moderate reducing conditions (Fig. 10). Representative electronic conductivity results are shown in Fig. 11 for the ceria-samaria system.

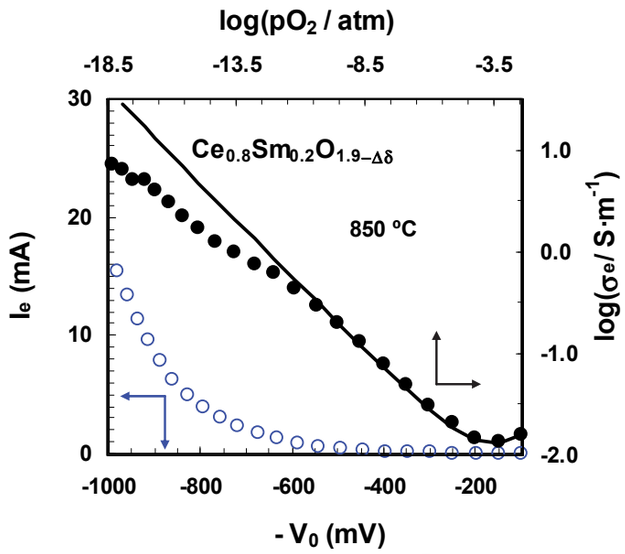


Fig. 10. Steady-state current-voltage curves for $Ce_{0.8}Sm_{0.2}O_{1.9-\Delta\delta}$ (open symbols) and corresponding electronic conductivity (closed symbols for secondary axes). The solid line represents $\pm 1/4$ power laws for the n- and p-type electronic conductivities (Eqs. 21 and 23).

Figure 11 shows that n-type electronic conductivity predominates under strongly reducing conditions, with a slight p-type electronic contribution for oxidising conditions. The decrease in contents of aliovalent additive increases the n-type electronic conductivity, mainly for moderately reducing conditions, due to the higher reducibility of the samples as argued in section 2.2. Moreover, the onset of p-type electronic conductivity is displaced towards higher $pO_2$ values, in good agree with the lower concentration of holes for samples with lower oxygen vacancy concentration under oxidising conditions, according to:

$$\frac{1}{2}O_2(gas) + V_O^{\bullet\bullet} \Leftrightarrow O_O^x + 2h^{\bullet} \quad (24)$$

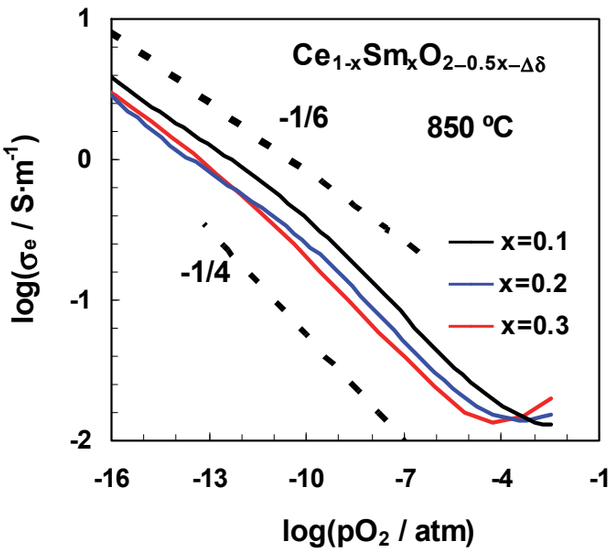


Fig. 11. Electronic conductivity versus oxygen partial pressure for $Ce_{1-x}Sm_xO_{2-0.5x-\Delta\delta}$ (x=0.1, x=0.2, x=0.3) extracted from differentiation of current-voltage curves given by Eq. 21.

Results of electronic conductivity under reducing conditions could be also analysed as function of temperature at fixed values of oxygen partial pressure (Eq. 20). Figure 12 shows results for ceria-samaria samples at $pO_2=10^{-10}$ atm.

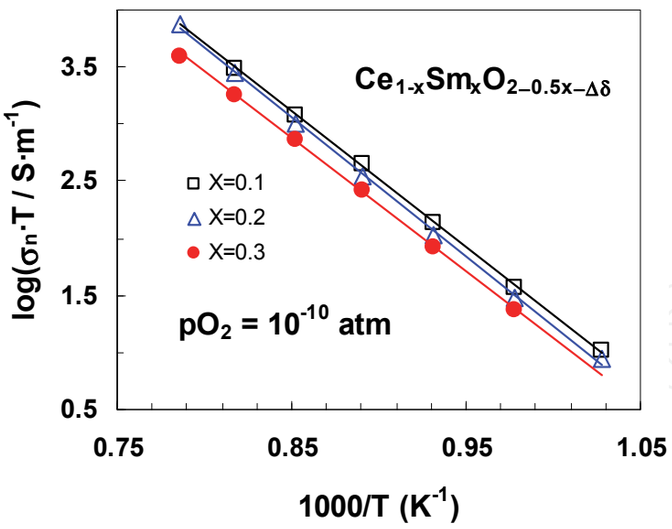


Fig. 12. Arrhenius plot of n-type electronic conductivity of ceria-samaria at $pO_2=10^{-10}$ atm.

The temperature dependence shown in Fig. 12 was used to estimate the activation energy of hopping of small polarons. Values in the range of 2.2-2.4 eV were obtained at $pO_2= 10^{-10}$ atm, which agree very well with our values of 2.3-2.4 eV previously reported for ceria-gadolinia (Pérez-Coll et al., 2007) and with those reported by other authors for cerias with different

lanthanides (Lübke & Wiemhofer, 1999; Steele, 2000; Xiong et al., 2004). According to Eq. 20 and using the results of enthalpy of reduction obtained in section 2.2 we have estimated values of activation energy for polaron mobility in the range 0.2-0.6 eV (Pérez-Coll et al., 2007).

The impact of reducibility of ceria-based solid electrolytes is determined mainly by the average transport number under high gradients of oxygen partial pressure, or corresponding dependence of average electronic conductivity on Nernst potential (Eq. 14) under steady-state conditions according to (Pérez-Coll et al., 2007):

$$\sigma_{e,av} = \frac{L}{A}\frac{I_e}{V_0} \tag{25}$$

Equation 25 directly relates the electronic conductivity with the voltage difference between both sides of the pellet. For this reason it describes the average electronic conductivity of the sample submitted to a difference of oxygen partial pressure (i.e. $pO_2^*$/ceria-sample/$pO_2$).

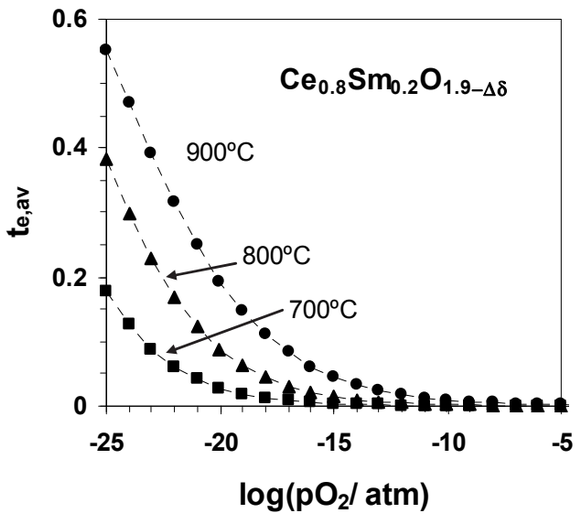


Fig. 13. Electronic transport number averaged across the mixed conducting membrane submitted to ion-blocking conditions as function of the oxygen partial pressure for $Ce_{0.8}Sm_{0.2}O_{1.9-\Delta\delta}$ at 700, 800 and 900 ºC

The electronic transport number could be averaged across the sample as follows:

$$t_{e,av} = \frac{\sigma_{e,av}}{\sigma_i + \sigma_{e,av}} \tag{26}$$

where $\sigma_i$ corresponds to ionic conductivity averaged across the membrane, which is usually assumed to be constant. Figure 13 shows an example of the effect of oxygen partial pressure and temperature on the averaged electronic transport number of $Ce_{0.8}Sm_{0.2}O_{1.9-\Delta\delta}$ estimated from ion-blocking and impedance spectroscopy results. The electronic character is revealed by substantial increase in the electronic transport number for very reducing conditions. However, due to the higher activation energy values for electronic conduction in the order

of 2.2-2.4 eV compared to those of ionic conduction in the order of 0.5-0.7 eV (Pérez-Coll et al., 2006) the averaged electronic transference number is decreased when temperature is lowered.

## 4. Fuel operating conditions

Previous sections emphasized that reduction of tetravalent cerium and thus the electronic conductivity in ceria based materials is highly influenced by the oxygen partial pressure. Under realistic situation in a SOFC the electrochemical reactions at the fuel electrode generate reaction products in the anode and corresponding changes in gas composition vs oxygen chemical potential (Frade et al. 2004). Thus interaction of the atmosphere with the anode materials and also with the contacting electrolyte surface will modify their electrical and electrochemical properties. In fact, one could expect different levels of fuel conversion along the anode surface that would be reflected in changes in the mixed transport properties of ceria-based materials, affecting the local performance of the SOFC due to non-uniform distribution of current density and corresponding heat management issues.

### 4.1 Dependence on conversion of hydrogen

The use of hydrogen as fuel in a SOFC produces water at the anode (for an oxide-ion conductor electrolyte) due to the reaction with the oxygen ions transported through the electrolyte and electronic transport in the external circuit (Fig. 14). Working conditions imposed by fuel conversion can be assessed by assuming nearly equilibrium for the overall reaction:

$$2\,H_2 + O_2 \Leftrightarrow H_2O \tag{27}$$

and corresponding mass action constant:

$$K = \frac{(pH_2O)^2}{pO_2\,(pH_2)^2} \tag{28}$$

where $pH_2O$, $pO_2$ and $pH_2$ are partial pressures of water, oxygen and hydrogen, respectively. Moreover, the relation between the equilibrium constant and the Gibbs free energy ($\Delta G$) is expressed as:

$$K = \exp\left(-\frac{\Delta G}{RT}\right) \tag{29}$$

Recombination of Eqs. 28-29 allows one to express the oxygen partial pressure as a function of steam to hydrogen ratio as follows:

$$pO_2 = \left(\frac{pH_2O}{pH_2}\right)^2 \exp\left(\frac{\Delta G}{RT}\right) \tag{30}$$

Equation 30 shows that local variations in steam to hydrogen ratio have considerable effects on the oxygen partial pressure.

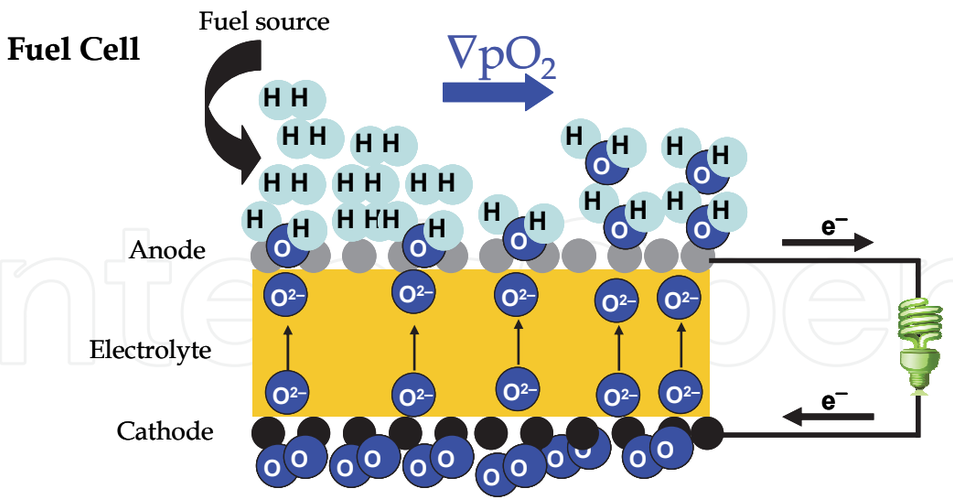


Fig. 14. Representation of a possible situation in a SOFC with different levels of conversion and different gas composition at the anode.

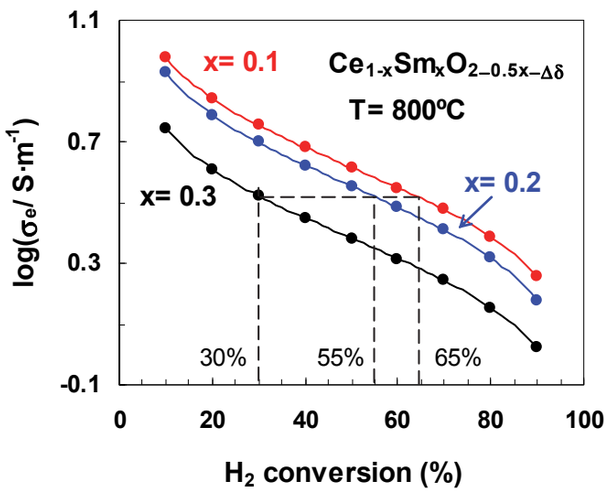


Fig. 15. Electronic conductivity in the reduced side of the samples as a function of the hydrogen conversion along the surface of the fuel side in the cell for a Sm-doped ceria system at 800 ºC.

Dependence of oxygen partial pressure on hydrogen conversion should, thus, be reflected in considerable changes in the electronic properties of ceria-based materials as illustrated in Fig. 15 for ceria-samaria electrolytes. The increase in the hydrogen conversion has the effect of lowering the electronic conductivity of the ceria-based materials as the atmosphere becomes less reducing. In extreme situations the electronic conductivity could be decreased by 5 to 6 times when the hydrogen conversion is increased from 10% to 90%. On the other hand, in spite of differences in electronic behaviour for samples doped with different contents of aliovalent cations, changes in hydrogen conversion may suppress the differences. The onset of electronic conductivity has also effects on the open cell voltage of

the mixed conducting membrane ($OCV_{mc}$), which can be estimated in a first approximation as:

$$OCV_{mc} \approx OCV_0 \left(1 - t_{e,av}\right) \tag{31}$$

where $OCV_0$ is the ideal open cell voltage for a pure ionic conductor (Eq. 14). Averaged electronic transport numbers of the mixed conducting membranes estimated from Eq. 26 could be recombinated with Eq. 30 to be represented as a function of the hydrogen:steam ratio (Fig. 16). It is observed that the increase in the $H_2$:$H_2O$ ratio increases considerably the electronic transference number, due to more severe reducing conditions, mainly at higher temperature and for lower values of Sm-content. Values of averaged transport number were also used to estimate the open cell voltage as function of hydrogen:steam ratio according to Eq. 31 and some results obtained at 700 ºC are represented in Fig. 17.

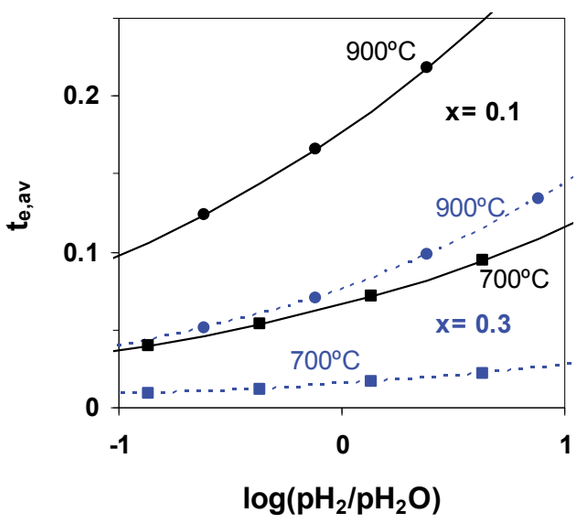


Fig. 16. Averaged electronic transport number at 700 and 900 ºC as a function of hydrogen:steam ratio in the mixture $H_2$+$H_2O$, for different Sm-contents in the system $Ce_{1-x}Sm_xO_{2-0.5x-\Delta\delta}$. [Continuous line: x= 0.1; dashed line: x=0.3)]

Figure 17 evidences that different mixtures of $H_2$+$H_2O$ produce important changes in the open cell voltage of the system. In spite of the relatively low temperature of 700 ºC, we can see substantial differences between the ideal open cell voltage and the current open cell voltage of the mixed conducting membrane. These differences are more important for higher values of $H_2$:$H_2O$ ratio and also for lower contents of trivalent dopant, according to the higher values of averaged electronic transport numbers (Fig. 16). Nevertheless, onset of mixed conductivity has recognized impact on electrocatalytic processes, which justifies its use in cermet anodes (Marina et al, 1999). Oxygen stoichiometry changes, and corresponding oxygen storage ability, may even contribute to minimize carbon deposition in those ceria-based anodes.

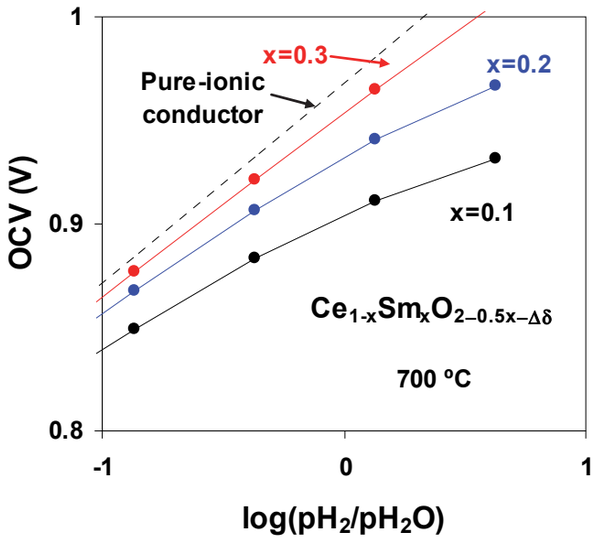


Fig. 17. Predictions of open cell voltage vs hydrogen:steam ratio for several contents of Sm in $Ce_{1-x}Sm_xO_{2-0.5x-\Delta\delta}$ at 700 ºC, based on the experimental dependence of electronic transport properties.

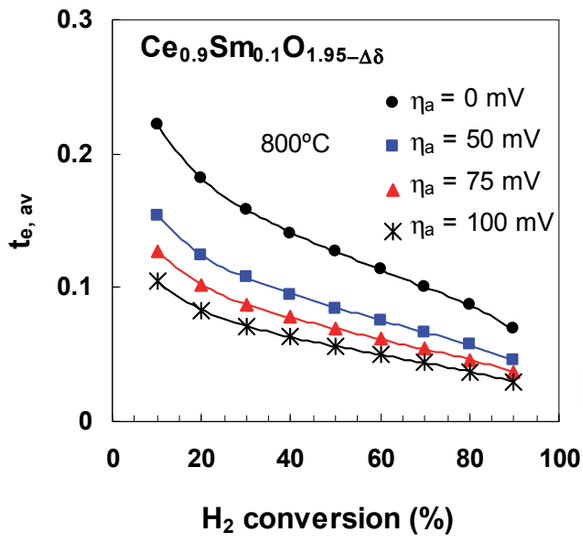


Fig. 18. Electronic transport number averaged across the membrane as function of hydrogen conversion for several values of anodic overpotential.

SOFC operation also yields overpotential contribution $\eta_a$ at the anode, and corresponding changes in actual reducing conditions imposed on materials exposed to fuels, i.e. (D. Pérez-Coll et al., 2010):

$$\eta_a = \frac{RT}{4F} \ln\left(\frac{pO_2}{pO_{2\text{-}R}}\right) \tag{32}$$

where the real oxygen partial pressure imposed on materials ($pO_{2\text{-}R}$) differs from the equilibrium oxygen partial pressure in the atmosphere (Eq. 30). Figure 18 shows the values of averaged electronic transport number as function of hydrogen conversion for different values of anodic overpotentials. It is highlighted that the increase in anodic overpotential decreases the averaged electronic transport number mainly for lower values of hydrogen conversion (higher reducing conditions). In fact, the current values of electronic transport number in the range 0.22-0.07 obtained at 800 ºC for hydrogen conversions in the range 10-90%, drops considerably to 0.1-0.03 under anodic polarisation, in the same range of conversion. Thus, differences in real working conditions change considerably the mixed conducting character of ceria-based compounds.

### 4.2 Dependence on conversion of methane

The use of methane as fuel produces more complex reactions and correlations between oxygen chemical potential and gas composition. (Frade et al., 2004). In this sub-section one will analyse the use of methane as fuel and the impact of conversion on the mixed transport properties. The thermodynamics of methane conversion may be analysed by a combination of partial oxidation to syngas:

$$CH_4 + \frac{1}{2}O_2 \Leftrightarrow CO + 2H_2 \qquad K_1 = \frac{pCO \cdot pH_2^{\,2}}{pO_2^{\,1/2} pCH_4} \tag{33}$$

with subsequent oxidation of CO and $H_2$ to fully oxidised species as follows:

$$CO + \frac{1}{2}O_2 \Leftrightarrow CO_2 \qquad K_2 = \frac{pCO_2}{pO_2^{\,1/2} pCO} \tag{34}$$

$$H_2 + \frac{1}{2}O_2 \Leftrightarrow H_2O \qquad K_3 = \frac{pH_2O}{pO_2^{\,1/2} pH_2} \tag{35}$$

where $K_1$, $K_2$ and $K_3$ are the equilibrium constants of corresponding equilibrium reactions and $p_i$ is the partial pressure of the corresponding species i. In real conditions, fuel conversion is preceded by steam reforming to minimize risks of methane cracking and corresponding blocking of gas channels and anode porosity. This also yields less reducing conditions and, thus, lower impact on OCV and electrochemical leaks. Actually, the equilibrium reaction under water vapor reforming could be expressed as:

$$CH_4 + H_2O \Leftrightarrow CO + 3H_2 \tag{36}$$

Equation 36 is a combination of Eqs. 33 and 35. Thus, reforming does not imply further changes in truly independent reactions required for thermodynamic analysis of methane conversion, and even contributes to validate the ideal assumption that methane cracking does not occur in fuel cell operation. The current procedure allows one to obtain partial pressures of different gas species as function of methane conversion ($\alpha$) and vs oxygen partial pressure with fixed values of starting steam:methane ratio ($w_0 = H_2O:CH_4$) (Frade et

al., 2004). A revision of this procedure has also been performed to account for conditions when carbon depositions are likely to occur. This extension combines the previous reactions with the equilibrium constant for methane cracking:

$$CH_4 \Leftrightarrow C(s)+2H_2 \tag{37}$$

and additional conditions for conservation of every elemental species (C, H and O). A representative example is shown in Fig. 19, for initial $H_2O:CH_4$=0.5:1 ratio, at 750ºC. A vertical dashed line shows the lowest level of oxidation oxygen:methane ratio required to ensure thermodynamic inhibition of carbon deposition. Note that this transition is also revealed by discontinuities in dependence of gas fractions on $O_2:CH_4$ ratio. Higher steam:metane ratio is, thus, needed to minimise risks of carbon deposition.

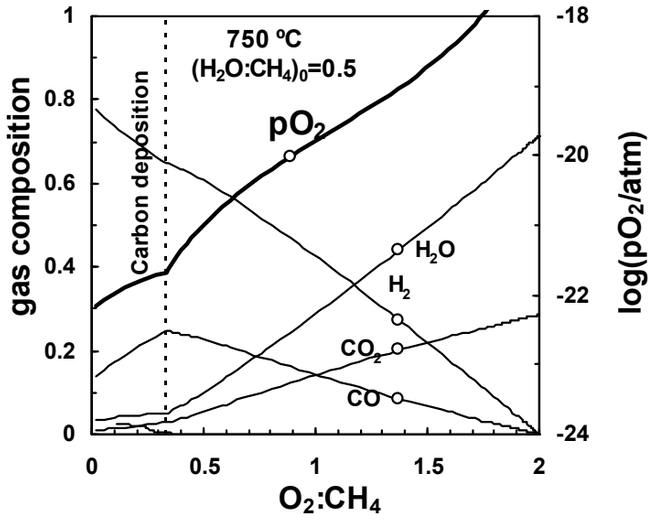


Fig. 19. Equilibrium gas composition (left vertical axis) and oxygen partial pressure (right vertical axis) at 750ºC as a function of oxygen:fuel ratio and with steam:methane ratio 0.5.

The dependence of the gas species on the oxygen partial pressure can be combined with the electronic properties of materials to obtain the electronic transport number as function of the fully oxidised species ($CO_2$ and $H_2O$). One example is shown in Fig. 20 for a $Ce_{0.8}Gd_{0.2}O_{1.9-\Delta\delta}$ sample at 750 ºC, with starting value $H_2O:CH_4$ = 1 and with several imposed values of anodic overpotentials. The increase in the content of fully oxidised species, and increasing anodic polarisation produces decrease of the electronic transport, thus lowering the impact of very reducing atmospheres. The analysis could be also performed paying attention to the effect produced by gradual oxidation on the cell voltage of the mixed conducting membrane. Figure 21 shows an example of the open cell voltage for $Ce_{1-x}Sm_xO_{2-0.5x-\Delta\delta}$ (x= 0.1, 0.2, 0.3) as a function of the contents of fully oxidised species. The increase of the concentration of these species reduces the open cell voltage, as expected for the decrease in oxygen chemical potential difference, with a moderate difference relative to the behaviour expected for a pure ionic conductor (Nernst potential). Yet, the contribution of this difference decreases gradually with increasing fuel oxidation, due to corresponding decrease in electronic conductivity. As a final consideration the values of open cell voltage

presented in this chapter may still deviate from the ideal behaviour for a solid electrolyte with residual electronic conductivity, due to the residual anodic polarisation caused by the internal current leakage (Frade et al., 2006 and 2008). As consequence the predictions for open cell voltage may still be somewhat overestimated, and the actual corrected solution should include these overpotential terms related to internal leakage:

$$OVC_{mc} = OCV_o(1-t_{e,av}) + \eta_{a,leak} + \left|\eta_{c,leak}\right| \quad (38)$$

where $\eta_{a,leak}$ and $\eta_{c,leak}$ are the anodic and cathodic overpotential contributions.

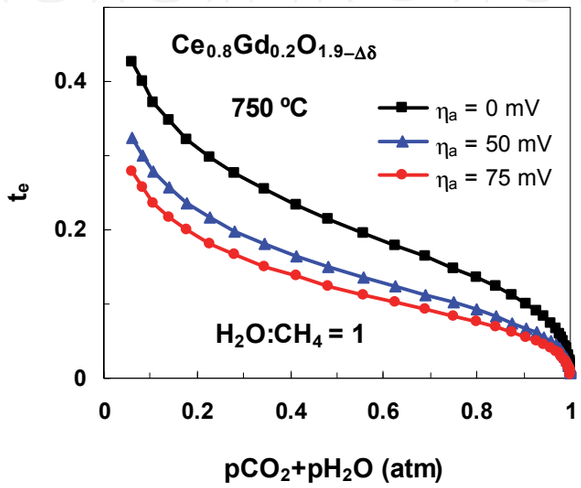


Fig. 20. Electronic transport number of $Ce_{0.8}Gd_{0.2}O_{1.9-\Delta\delta}$ at 750 ºC vs. fraction of fully oxidised species ($CO_2$ and $H_2O$) for $\eta_h$ = 0, 50 and 75 mV, with initial $H_2O$:$CH_4$ = 1:1.

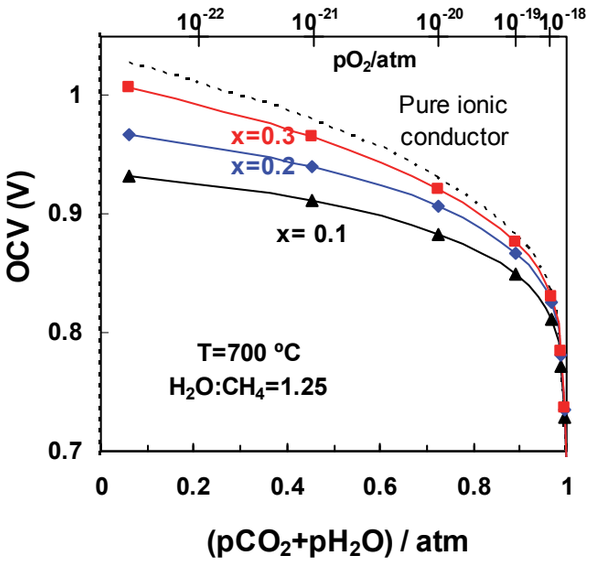


Fig. 21. Open cell voltage at 700 ºC as function of the content of $pO_2$+$pH_2$ for $Ce_{1-x}Sm_xO_{2-0.5x-\Delta\delta}$ system (x= 0.1, 0.2, 0.3) and for a starting steam:methane ratio 1.25.

## 5. Constraints imposed by chemical expansion

Reduction from $Ce^{4+}$ to $Ce^{3+}$ also causes lattice expansion, and risks of significant stresses under high gradients of chemical potential (Atkinson & Ramos, 2000). Chemical expansion is usually correlated to oxygen stoichiometry changes relative to air (reference conditions), and described by the chemical expansion coefficient $\varepsilon'_C = \Delta\varepsilon/\Delta\delta$. Representative results are shown in Fig. 22. One can see that cerias often show quite higher chemical expansion coefficient than typical perovskite mixed conductors such as LSCF (Lein et al, 2006). On combining the chemical expansion coefficient with the dependence of oxygen stoichiometry on oxygen:fuel ratio, and overpotential one obtained the results shown in Fig. 23. For very low fuel conversion and low anodic polarisation this yields a strain contribution in the order of 0.6%. Indeed, chemical strain may also contribute to the enhanced redox tolerance of Ni-CGO cermet anodes (Ouweltjes et al, 2009), as chemical contraction of CGO may provide compensation for expansion caused by partial oxidation of Ni to NiO.

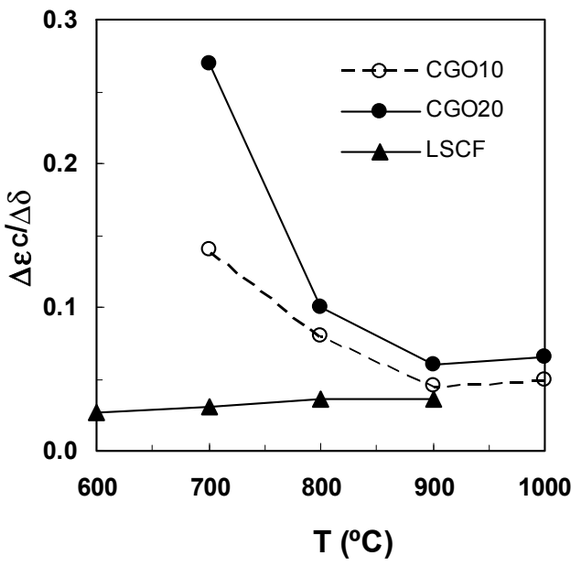


Fig. 22. Representative results of chemical expansion coefficient of $Ce_{0.9}Gd_{0.1}O_{2-\delta}$ (CGO10), $Ce_{0.8}Gd_{0.2}O_{2-\delta}$ (CGO20) (Atkinson & Ramos, 2000), and $La_{0.5}Sr_{0.5}Fe_{0.5}Co_{0.5}O_{3-\delta}$ (LSCF) (Lein et al, 2006).

In order to assess the impact of chemical expansion on thermochemical stresses one may combine chemical strain $\varepsilon_C(x)$ superimposed on a stress related contribution, in flat constrained conditions as follows:

$$\varepsilon_\gamma = \sigma(x)(1-\nu)/E + \varepsilon_C(x) \tag{39}$$

where $\sigma(x)$ denotes stress, E is Young modulus and $\nu$ is the Poisson ratio.

For flat constrained conditions, the resulting strain $\varepsilon_\gamma$ remains uniform across the membrane, and thus:

$$\sigma(x) = \frac{E}{(1-\nu)}\left[\varepsilon_\gamma - \varepsilon_C(x)\right] \tag{40}$$

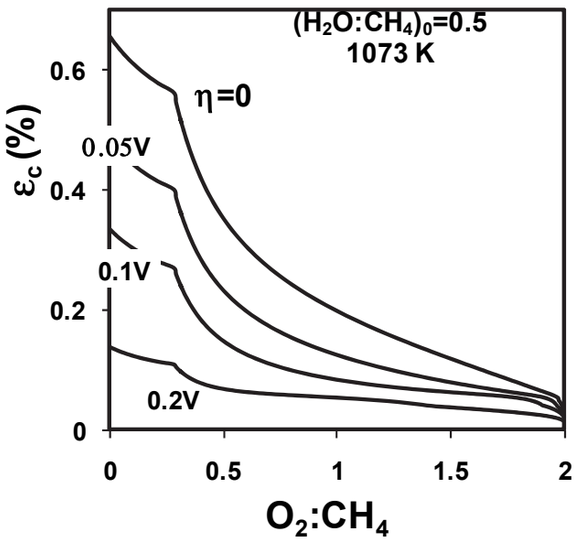


Fig. 23. Chemical expansion of CGO20 vs $O_2$:$CH_4$ ratio for $(H_2O:CH_4)_0$=0.5, at 800°C, and for anodic polarisation η=0, 0.05, 0.1, 0.2 V.

This can be combined with the additional condition for externally unconstrained membranes:

$$\int_0^L \sigma dx \approx \frac{L}{\Delta\mu O_2} \int_{\mu O_2'}^{\mu O_2''} \sigma d\mu O_2 = 0 \tag{41}$$

where L is the thickness of membrane, and $d\mu O_2 = RTd\ln(pO_2)$ is the elemental change in chemical potential. For linear dependence of chemical potential across the membrane, and on combining Eqs. 40 and 41 one obtains:

$$\varepsilon_\gamma = \log\left(pO_2'' / pO_2'\right)^{-1} \int_{pO_2'}^{pO_2''} \varepsilon_C d\log(pO_2) \tag{42}$$

If x represents distance from air, and this is taken as reference, i.e. $\varepsilon_c(0)=0$, the stresses at surfaces in contact with air x=0 and contact with fuel (x=L) become:

$$\sigma(0) = \frac{E\,\varepsilon_\gamma}{(1-\nu)} \tag{43}$$

$$\sigma(L) = \frac{E\left(\varepsilon_\gamma - \varepsilon_C(L)\right)}{(1-\nu)} \tag{44}$$

Dependence on oxygen partial pressure is then easily transformed to the corresponding conversion of fuels, based on the previous thermodynamic analysis for hydrogen or methane-based fuels.

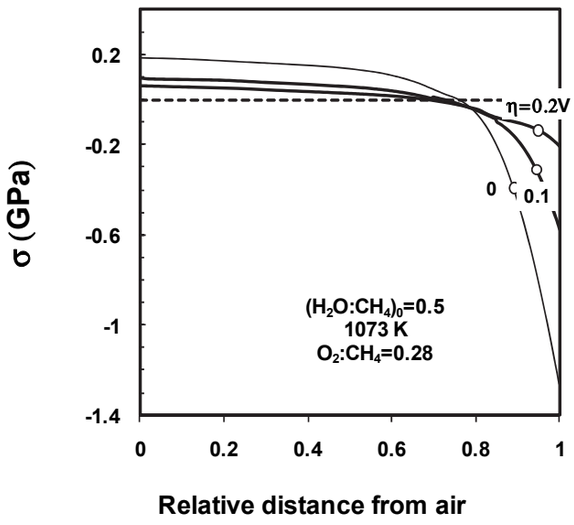


Fig. 24. Predictions of stresses in a CGO20 membrane vs. relative distance to air, under air/membrane/fuel conditions with $(H_2O:CH_4)_0$=0.5, at the lowest conditions to avoid carbon deposition $O_2:CH_4$≈0.28, and for different anodic overpotentials η=0, 0.1, and 0.2V.

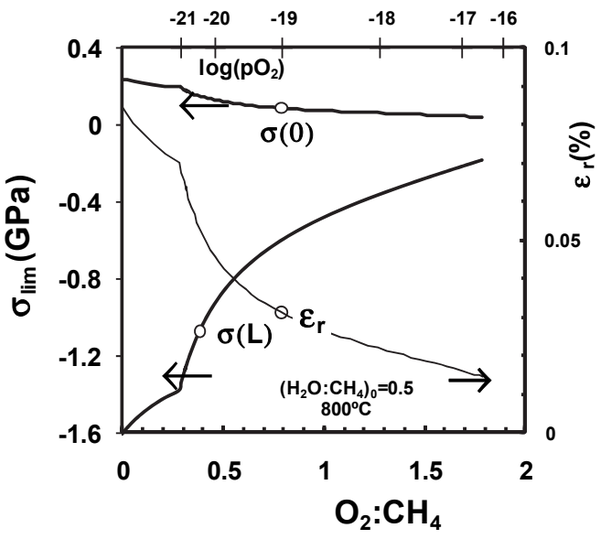


Fig. 25. Predicted dependence of overall chemical strain and stresses induced by chemical expansion at the air side σ(0) and at the fuel side σ(L) versus oxygen:fuel ratio, at 800ºC and for the initial steam methane ratio = 0.5.

On combining with corresponding dependence of oxygen sub-stoichiometry on $pO_2$, for typical values of chemical expansion coefficient, one estimated the stress profiles across a ceria based membrane for representative conditions, as shown in Fig. 24, using also the values of parameters E=187 GPa and ν=0.334 reported by (Atkinson & Selçuk, 2000). Note that slightly tensile stresses develop at the oxidising side and much higher compressive stresses at reducing side. This is, probably, the most favourable condition because ceramics show much higher resistance under compression. Still, relatively high chemical expansion in contact with the fuel may still raise risks of delaminating at ceria/electrode contacts. Figure 25 shows additional results for the dependence of stresses in contact with air σ(0) and in contact with the fuel σ(L), vs. oxygen:methane ratio in the feed, or upon the gradual oxidation. The discontinuities in overall strain and stresses in contact with air or contact with fuel represent the minimum oxidation required to avoid carbon deposition.

## 6. Conclusions

Partial reducibility of ceria-based materials exposed to fuels or other reducing agents causes onset of significant electronic conductivity, decrease in oxygen stoichiometry and chemical expansion. These changes are closely dependent on oxygen partial pressure and can also be related to gradual conversion of fuels until nearly complete conversion to fully oxidised gases (i.e. $H_2O$ and/or $CO_2$); this can be described by thermodynamic analysis of fuel conversion, yielding a description for effects on electronic conductivity, changes in oxygen stoichiometry and chemical strain. Fuel rich atmospheres yields mixed conducting properties, with negative impact on electrolytic domain and open circuit voltage (OCV) for a ceria-based membrane under air/membrane/fuel gradients. For this configuration, one must consider the average value of electronic conductivity across the membrane to account for effects on OCV. Simultaneously, the gradient of chemical potential yields variable oxygen stoichiometry across the ceria-based membrane, and corresponding chemically induced stresses. Under flat constrained conditions, stresses may change gradually from moderate tensile stresses, in the air side, to compressive stresses in the fuel side. Thus, onset of electronic conductivity and chemical expansion may impart operation conditions for ceria-based solid electrolytes. Yet, reducibility may also confer unique electrocatalytic properties to ceria-based materials, and applicability in cermet anodes due to mixed conductivity, possibly combined with variable oxygen storage. In addition, one may anticipate enhanced redox tolerance for ceria-based cermet anodes, as chemical contraction of the ceria-based component upon reoxidation may counter expansion induced by partial oxidation of metallic Ni to NiO.

## 7. Acknowledgment

This work was sponsored by MCINN (Spain) (ENE2009-14750-C05-03) and co-financed by FEDER-EU (MAT2007-60127 and MAT2010-16007). Domingo Pérez-Coll is also grateful to MCINN and CSIC for a "Ramón y Cajal" contract.

## 8. References

Abrantes J.C.C., Pérez-Coll D., Núñez P., Frade J.R., *Electrochim. Acta*, 48 (2003) 2761

Atkinson A., Ramos T.M.G.M., *Solid State Ionics*, 129 (2000) 259
Atkinson A., Selçuk A., *Solid State Ionics*, 134 (2000) 59
Butler, V.; Catlow, C.R.A.; Fender, B.E.F.; Harding, J.H.; *Solid State Ionics,* 8 (1983) 109
Blumenthal, R.N.; Hofmaier, R.L. *J. Electrochem.Soc* 121 (1974) 126
Blumenthal, R.N.; Sharma, R.K.; *J. Solid State Chem*. 13 (1975) 360.
Catlow, C.R.A.; *Solid State Ionics* 8 (1983) 89
Fagg, D.P.; Abrantes, J.C.C.; Pérez-Coll, D.; Núñez, P.; Kharton,V.V.; Frade, J.R.; *Electrochim. Acta*, 48 (2003) 1023-1029
Ferreira, A.A.L.; Abrantes, J.C.C.; Jurado, J.R.; Frade, J.R.; *Solid State Ionics*, 135 (2000) 761
Frade, J. R.; Kharton, V.V.; Yaremchenko, A.; Naumovich, E.; *J. Power Sources,* 130 (2004) 77
Frade, J. R.; Kharton, V.V.; Yaremchenko, A.A.; Tsipis, E.V.; *J. Solid State Electrochem.*, 10 (2006) 96-103
Frade, J. R.; Kharton, V.V.; Shaula, A.L.; Maques, F.M.B.; *Sensor Letters.*, 6 (2008) 370-380
Hebb, M.H.; J. Chem. Phys. 20 (1952) 185
Kobayashi, T.; Wang, S.; Dokiya, M.; Tagawa, H.; Hashimoto, T.; *Solid State Ionics,* 126 (1999) 349
Lein H.L., Wiik K., Grande T., *Solid State Ionics,* 177 (2006) 1795
Lübke, S.; Wiemhoefer, H.-D.; *Solid State Ionics,* 117 (1999) 229
Marina O.A., Bagger C., Primdahl S., Mogensen M., *Solid State Ionics,* 123 (1999) 199
McIntosh S., Gorte R.J., *Chem. Rev*., 104 (2004) 4845
Minervini, L.; Zacate, M.O.; Grimes, R.W.; *Solid State Ionics,* 116 (1999) 339
Mogensen, M.; Sammes, N.M.; Tompsett, G.A.; *Solid State Ionics,* 129 (2000) 63
Navarro, L.; Marques, F.; Frade, J.R.; *J. Electrochem. Soc*, 144 (1) (1997) 267
Ouweltjes J.P., van Tuel M., Sillessen M., Rietveld G., *Fuel Cells,* 9 (2009) 873
Panhans, M. A.; Blumenthal, R. N.; *Solid State Ionics,* 60 (1993) 279
Pérez-Coll D., Núñez P., Marrero-López D., Abrantes J.C.C., Frade J.R., *J. Solid State Electrochem*., 8 (2004) 644
Pérez-Coll D., Núñez P., Frade J.R., *J. Electrochem. Soc.,* 153 (3) (2006) A478
Pérez-Coll D., Marrero-López D., Ruiz-Morales J.C., Núñez P., Abrantes J.C.C., Frade J.R., *J. Power Sources*, 173 (2007) 291
Pérez-Coll D., Aguadero A., Núñez P., Frade J.R., *Int. J. Hydrog. Energy*, 35 (2010) 1148
Riess, I. ; Janczikowski; Nölting, J.; *J. Appl. Phys*., 61 (1987) 4931
Schneider, D.; Godickemeier, M.; Gauckler, L.J.; *J. Electroceramics,* 1 (1997) 165
Steele, B.C.H.; *Solid State Ionics*, 129 (2000) 95-110
Suzuki,T.; Kosacki, I,; Anderson, H.U.; *J. Am. Ceram. Soc*., 85 (2002) 1492
Tikhonovich, V.N.; Naumovich, E.N.; Kharton, V.V.; Yaremchenko, A.A.; Kovalevsky, A.V.; Vecher, A.A.; *Electrochim. Acta*, 47 (2002) 3957
Tsipis E.V., Kharton V.V., Bashmakov I.A., Naumovich E.N., Frade J.R., *J. Solid State Electrochem*., 8 (2004) 674
Tuller, H.L.; Nowick, A.S.; *J. Phys. Chem. Solids*, 38 (1977) 859
Wagner, C.; Proceedings of the Seventh Meeting of the International Committee on Electrochemical Thermodynamics and Kinetics, Lindau, Butterworths Scientific Publication, London, (1957), p. 361
Wang, S. R.; Inaba, H.; Tagawa, H.; Hashimoto, T.; *J. Electrochem. Soc*.,144 (1997) 4076

Wang, S.R.; Inaba, H.; Tagawa, H.; Dokiya, M.; Hashimoto, T.; *Solid State Ionics,* 107 (1998) 73
Xiong, Y.; Yamaji, K.; Horita, T.; Sakai, N.; Yokokawa, H.; *J. Electrochem. Soc.*, 151 (2004) A407
Yano, M., Tomita A., Sano M., Hibino T., *Solid State Ionics*, 177 (2007) 3351
Zachau-Christiansen B.; Jacobsen, T.; Skaarup, S.; *Solid State Ionics*, 86-88 (1996) 725

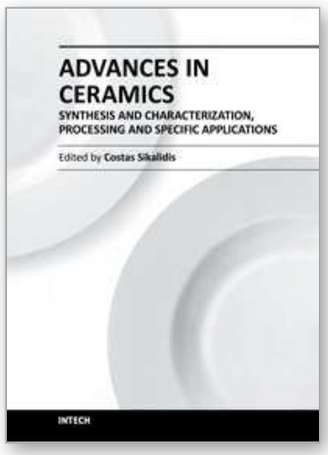


**Advances in Ceramics - Synthesis and Characterization, Processing and Specific Applications**

Edited by Prof. Costas Sikalidis

ISBN 978-953-307-505-1
Hard cover, 520 pages
**Publisher** InTech
**Published online** 09, August, 2011
**Published in print edition** August, 2011

The current book contains twenty-two chapters and is divided into three sections. Section I consists of nine chapters which discuss synthesis through innovative as well as modified conventional techniques of certain advanced ceramics (e.g. target materials, high strength porous ceramics, optical and thermo-luminescent ceramics, ceramic powders and fibers) and their characterization using a combination of well known and advanced techniques. Section II is also composed of nine chapters, which are dealing with the aqueous processing of nitride ceramics, the shape and size optimization of ceramic components through design methodologies and manufacturing technologies, the sinterability and properties of ZnNb oxide ceramics, the grinding optimization, the redox behaviour of ceria based and related materials, the alloy reinforcement by ceramic particles addition, the sintering study through dihedral surface angle using AFM and the surface modification and properties induced by a laser beam in pressings of ceramic powders. Section III includes four chapters which are dealing with the deposition of ceramic powders for oxide fuel cells preparation, the perovskite type ceramics for solid fuel cells, the ceramics for laser applications and fabrication and the characterization and modeling of protonic ceramics.



**InTech Europe**
University Campus STeP Ri
Slavka Krautzeka 83/A
51000 Rijeka, Croatia
Phone: +385 (51) 770 447
Fax: +385 (51) 686 166
www.intechopen.com

**InTech China**
Unit 405, Office Block, Hotel Equatorial Shanghai
No.65, Yan An Road (West), Shanghai, 200040, China
中国上海市延安西路65号上海国际贵都大饭店办公楼405单元
Phone: +86-21-62489820
Fax: +86-21-62489821

IntechOpen